

Minh-Thai LE¹

An-Le VAN^{2*}

Trung Thanh NGUYEN³

PERFORMANCE OPTIMIZATION OF MULTI-ROLLER FLAT BURNISHING PROCESS IN TERMS OF SURFACE PROPERTIES

In the current investigation, two primary indicators, including the average roughness (*AR*) and Brinell hardness (*BH*) of the roller burnishing operation are enhanced using the optimal inputs (the spindle speed-*S*, feed rate-*f*, and depth of penetration-*D*). The performance measures are developed using the Kriging approach and optimal outcomes are generated by the Crow Search Algorithm (CSA). The optimal outcomes generated by the CSA of the *S*, *f*, and *D* were 832 rpm, 112 mm/min, and 0.12 mm, while the *AR* was reduced by 37.0% and the *BH* was increased by 29.9%, respectively. The optimal findings could be utilized in the practice for enhancing the burnished quality and to develop a professional system related to the roller burnishing operation. The Kriging-based *AR* and *BH* correlations could be used to present nonlinear experimental data. The optimizing technique could be utilized to deal with optimizing problems for different machining operations.

1. INTRODUCTION

The roller burnishing operation is extensively utilized to produce flat and internal surfaces with high quality, in which the pressure of the rollers is utilized to compress the material. The excessive pressure of the roller helps to reduce the irregularities, boost the hardness as well as the effective stress, and increase the production rate, as compared to the ball-burnishing one. This operation can be utilized for machining ferrous and non-ferrous materials in single and mass productions. Therefore, the roller burnishing operation is an effective solution to fabricate machined components with high quality.

A set of attempts has been conducted to improve the technical performances of different roller burnishing operations. The empirical models of the average roughness (*AR*) and Vickers hardness (*VH*) were proposed in terms of the burnishing force (*BF*), feed rate (*f*), width (*W*), and the number of passes (*NP*) [1]. The authors stated that the *AR* was decreased

¹ Faculty of Special Equipments, Le Quy Don Technical University, Vietnam

² Faculty of Engineering and Technology, Nguyen Tat Thanh University, Vietnam

³ Faculty of Mechanical Engineering, Le Quy Don Technical University, Vietnam

* E-mail: lvan@ntt.edu.vn

<https://doi.org/10.36897/jme/161661>

by 95% and the *VH* was improved by 12% at the selected optimality. Patel and Brahmhatt presented that the *f* was found to be the most effective parameter on the *AR* model of the burnished AA6061 [2]. John et al. emphasized that the *S* of 1100 rpm, *f* of 0.11 mm/rev, and penetration allowances of 0.03 mm could be applied to decrease the *AR*, ovality, and bore size of the internal burnished cast iron [3]. Yuan et al. emphasized that higher values of the *S* and *D* were applied to enhance the *AR* and *VH* responses [4]. Shankar et al. indicated that the coated roller could be applied to decrease the *AR* of the burnished composite in the dry condition [5]. Nguyen et al. stated that the *AR* of 0.071 μm and the Rockwell hardness of 52 HRC could be obtained using the optimal *S*, *f*, and *D* for the burnished carbon steel [6]. The *AR*, cylindricity (*CL*), and circularity (*CC*) were saved by 55.0%, 80.0%, and 2.0% at the optimal *S*, *f*, and *D* for the burnished hardened steel [7]. The ANFIS models of the energy efficiency and machining noise were developed regarding the *S*, *f*, *D*, and the number of rollers for internal burnished SCr440 steel [8]. The authors stated that the energy efficiency and machining noise were saved by 7.0% and 2.2% at the optimality. The enhancements in the maximum profile peak height of the roughness (*MAR*) and the *VH* of the burnished carbon steel were 17.0% and 14.0%, respectively, using the optimal operating parameters of the minimum quantity lubrication (MQL) system [9]. Duncheva et al. presented that the fatigue life of the 2024-T3 Al could be improved by more than 2000 times with the support of the single toroidal roller burnishing [10]. The total energy consumption (*TE*), mean roughness depth (*MR*), and *CC* models of the MQL-assisted burnishing operation were proposed in terms of the *S*, *D*, flow rate (*F*), and inlet pressure (*P*) [11]. The authors stated that *TE*, *MR*, and *CC* were decreased by 12.2%, 14.2%, and 42.5%, respectively at the optimality. The predictive models of the *AR*, *VH*, and *CC* were developed in terms of the *S*, *f*, *BF*, and *NP*, respectively for the burnished magnesium. The authors stated that the optimal values of the *S*, *f*, *BF*, and *NP* were 171 rpm, 0.18 mm/rev, 21 N, and 3 [12]. The MQL parameters, including the diameter of the nozzle diameter, elevation angle, *F*, and *P* were optimized to decrease the *CL* and *CC* of the burnished hole [13]. The authors stated that the *CYL* and *CIC* were decreased by 53.14% and 72.97%, respectively. However, the shortcomings of the aforementioned works can be expressed as:

The predictive models of the *AR* and *BH* for the roller burnishing process have been not presented in published works.

Additionally, the selection of optimal process parameters for minimizing *AR* and maximizing *BH* of the roller burnishing process has been not addressed in the previous works.

To save experimental costs and human efforts, it is necessary to propose an effective technique, which can save human efforts and find the best outcomes.

In this paper, we present optimization steps and experiment setting for the roller burnishing process of the hardened steel. Next, the obtained results are scientifically discussed. Finally, conclusions are drawn and future research is suggested.

2. OPTIMIZATION APPROACH

The optimization approach is presented in Fig. 1.

Step 1: Generating experimental outcomes using the Box-Behnken method.

The Box-Behnken method is an effective design of the experiment, in which each factor with three levels ($-1, 0, +1$) presents the lowest, middle, and highest ranges. The design points are assigned on the center and edge of the block. This approach decreases the number of experiments, leading to reduction in the costs and human efforts. The number of experiments (NE) in the Box-Behnken method is calculated as:

$$NE = 2k(k - 1) + C_p \quad (1)$$

where k and C_p present the number of parameters and the number of center points, respectively. In this work, three process parameters having three levels and three center points are employed; hence, 17 experiments are generated.

The AR is calculated as:

$$AR = \frac{\sum_{i=1}^n Ra_i}{n} \quad (2)$$

where Ra_i is the average roughness at the i_{th} measured location.

The BH is calculated as:

$$BH = \frac{\sum_{i=1}^n BH_i}{n} \quad (3)$$

where BH_i is the Brinell hardness at the i_{th} measured location.

Step 2: The Kriging-based AR and BH models are developed.

The interpolative Kriging correlation is expressed as:

$$y(x) = \beta f(x)^T + Z(x) \quad (4)$$

where x , $\beta f(x)^T$, and $Z(x)$ are HSPRT variables, regressive coefficients, and errors, respectively. The covariance- $Z(x)$ in the design scope is computed as:

$$\text{cov}(Z(x_a), Z(x_b)) = \sigma_z^2 R(x_a, x_b) \quad (5)$$

where σ_z^2 and $R(x_a, x_b)$ are the dissimilarity and correlative functions, respectively.

The σ_z^2 is computed as:

$$\sigma_z^2 = \frac{1}{N} (Y - \beta X)^T R^{-1} (Y - \beta X) \quad (6)$$

where $X = [f(x_1), f(x_2), \dots, f(x_N)]^T$ and Y denote the response vector of the samples.

The $R(x_a, x_b)$ is computed as:

$$R(x_a, x_b) = \exp\left[-\sum_{i=1}^d \theta_i (x_{ai} - x_{bi})^2\right] \quad (7)$$

where d and θ_i are the dimension and undetermined parameter, respectively.

The θ_i is computed as:

$$\min_{\{\theta_1, \theta_2, \dots, \theta_N\}} \left\{ \left| R \left[\frac{1}{N} \sigma_z^2 \right] \right\} \quad (8)$$

where $|R|$ is the determinant of the correlation matrix R .

The β is computed as:

$$\beta = (X^T R^{-1} X)^{-1} (X^T R^{-1} Y) \quad (9)$$

The predictive correlation is expressed as:

$$\hat{y}(x^*) = f(x^*)^T \beta + r(x^*)^T R^{-1} (Y - X\beta) \quad (10)$$

where the vector $r(x^*)^T = [R(x^*, x_1) R(x^*, x_2) \dots R(x^*, x_N)]$.

The predictive error (ER) is calculated as:

$$ER = \frac{Ex - Pd}{Ex} \quad (11)$$

where Ex and Pd are the experimental and predictive outcomes, respectively.

Step 3: The CSA is utilized to find optimal outcomes

The CSA is an efficient optimization approach, which is inspired by the behaviour of crows to hide and find the food. The crow can follow another one to obtain a better food and it will try to change the place of its food. The working procedure of the CSA is depicted in Fig. 2:

- Initializing the population size (p), iteration number (t), flight step size (fz), and awareness probability (ap).

- The individual crows and memory matrix are produced in the design space. The position matrix presents the position of the i_{th} crow, in which each crow $x_i = (X_{i,1}, X_{i,2}, \dots, X_{i,d})$ presents a feasible problem. The memory matrix describes the best position of the i_{th} crow, in which the position of each crow is given by a vector $m_i = (M_{i,1}, M_{i,2}, \dots, M_{i,d})$.

- Evaluation of the quality of each crow based on the fitness function.

- Generation of a new location for each crow in the design space. The updated position of the i_{th} crow can be expressed in two situations:

If j_{th} crow does not observe that the i_{th} crow is following it. In this case, the updated position of the j_{th} crow is expressed as:

$$x^{i,t+1} = x^{i,t+1} + r_i + fz^{i,t} \times (m^{i,t} - x^{i,t}) \quad (12)$$

If j_{th} crow observes that the i_{th} crow is following it. In this case, the updated position of the j_{th} crow is expressed as:

$$x^{i,t+1} = x^{i,t+1} + r_i + fz^{i,t} \times (m^{i,t} - x^{i,t}), r_j \geq ap \quad (13)$$

where r_i is a random number with a uniform distribution between 0 and 1.

- Evaluation of a new position of each individual. If an updated location is feasible, a crow has been observed a new position.

- Calculation of the fitness value of the new position of each crow.

- The memory matrix of each crow is updated.

Table 1 presents the burnishing factors and their ranges. The values of the spindle speed and feed rate are determined based on the specifications of the CNC machine. These values

are confirmed by the recommendations of the manufacturer of the burnishing tool. The ranges of the depth of penetration are selected using the configuration of the burnishing tool. A set of trials was performed at the minimum and maximum values of the process inputs to ensure machinability.

Table 1. Process inputs of the roller burnishing process

Symbol	Parameters	Unit	Ranges
S	Spindle speed	Rpm	400-800-1200
f	Feed rate	mm/min	100-300-500
D	Depth of penetration	mm	0.04-0.08-0.12

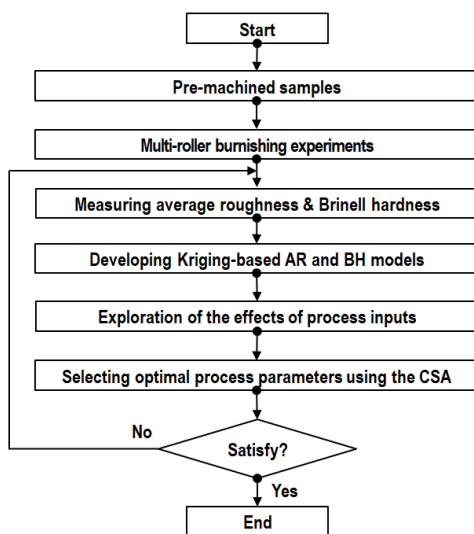


Fig. 1. The optimizing approach

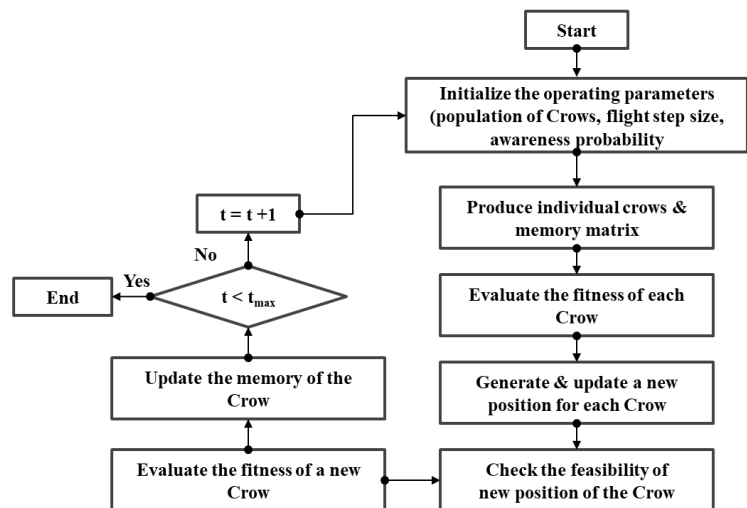


Fig. 2. The working principle of the CSA

3. BURNISHING EXPERIMENTS

A CNC milling device entitled SPINNER U-620 is utilized to perform the experimental trials (Fig. 3a). The specifications of the machine tool are presented in Table 2. The burnishing tool is tightly clamped on the spindle system, while the precision vise is applied to fix the workpiece. The burnishing tool having three changeable rollers is utilized and a new roller is used for each trial. Table 3 presents the specifications of the burnishing tool. The flood condition is employed to facilitate all experiments.

The length, width, and height of each specimen are 72.0 mm, 22.0 mm, and 12.0 mm, respectively. The hardened steel entitled AISI 5150 is chosen because of extensive employment in the automotive sector. The chemical compositions of the AISI 5150 are presented in Table 4. The rough milling using a tool with a diameter of 60 mm and three inserts is utilized to produce the pre-burnished surface. The milling conditions, including the spindle speed of 500 rpm, feed rate of 120 mm/min, and depth of cut of 0.5 mm are applied. The average

roughness and Brinell hardness of the milled surface are 2.46 μm and 275 HB. The burnished samples are shown in Fig. 3b.

The Brinell hardness is observed with the support of an Ernst hardness tester (Fig. 3c), while a Mitutoyo SJ-301 is utilized to capture the roughness profile and value (Fig. 3d).

The representative values of the *AR* and *BH* responses are presented in Fig. 4.

Table 2. The specifications of the machine tool

Parameters	Unit	Ranges
X, Y, and Z travels	mm	620, 520, and 460
Table surface area	mm ²	800
Controller		FANUC
Spindle speed	rpm	60-9000
Spindle taper		SK 40
Maximum table load	kg	500
Maximum weight of tool	kg	7.0
ATC	Position	30
Total power requirement	kVA	30
Weight of the machine	Ton	6.9
Length x Weight x Height	m	2.6 x 2.35 x 2.75



(a) Preparing samples on CNC milling centre



(b) Samples after machining



(c) Measuring surface hardness



(d) Measuring surface roughness

Fig. 3. Experimental setting for the roller burnishing process

Table 3. The specifications of the burnishing tool

Parameters	Unit	Ranges
Outside diameter	mm	41.8
Working diameter	mm	22
Inner diameter	mm	20
Length of shank	mm	60
Total length	mm	85
Number of rollers	Piece	3
Maximum rotational speed	rpm	3500
Maximum feed rate	mm/rev.	0.8
Maximum depth of penetration	mm	0.16
Minimum depth of penetration	mm	0.02
Total power requirement	kVA	30
Weight of the machine	Ton	6.9
Length×Weight×Height	m	2.6×2.35×2.75

Table 4. Chemical compositions of AISI 5150 alloy steel

Elements	Mn	Cr	C	Si	S	P	Fe
%	0.80	0.80	0.52	0.20	0.04	0.035	balance

4. RESULTS AND DISCUSSIONS

4.1. ANOVA ANALYSIS

The experimental outcome and parametric values of Kriging models are shown in Tables 5 and 6, respectively. The ANOVA is applied to investigate the significance of the model and effective parameters [14, 15].

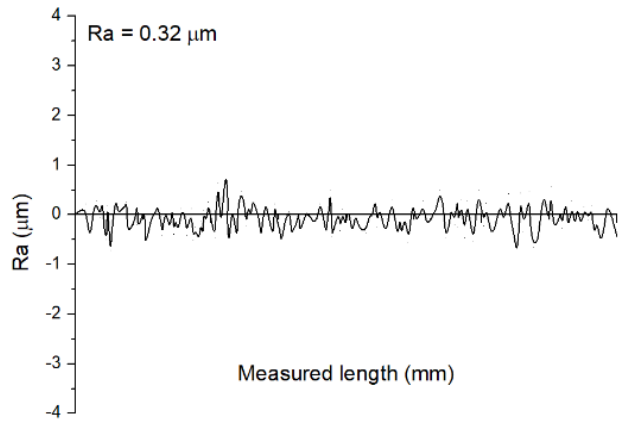
The ANOVA results of the *AR* are presented in Table 7. Significant factors are single factors (S , f , and D) and quadratic factors (S^2 and f^2) (Fig. 5a). The contributions of the S , f , and D are 4.74%, 21.98%, and 19.84%, respectively. The contributions of the S^2 and f^2 are 38.79% and 12.93%, respectively. The values of the R^2 value (0.9782), Adjusted R^2 (0.9702), and Predicted R^2 (0.9672) indicate that the *AR* model is adequate.

The ANOVA results of the *BH* are presented in Table 8. Significant parameters are single factors (S , f , and D), interactive factors (SD and fD), and quadratic factors (S^2 , f^2 , and D^2) (Fig. 5b). The contributions of the S , f , and D are 19.64%, 19.17%, and 20.89%, respectively. The contributions of the SD and fD are 6.76 and 3.24%, respectively. The contributions of the S^2 , f^2 , and D^2 are 5.26%, 7.32%, and 14.64% respectively. The values of the R^2 value (0.9814), the Adjusted R^2 (0.9754), and the Predicted R^2 (0.9646) indicate that the *BH* model is adequate.

To evaluate the precision of Kriging models, experiments at random points are executed. The deviations between the actual and predictive values of the *AR* and *BH* lie from -4.00% to 5.26% and -0.71% to 0.53% , respectively (Table 9), presenting the acceptable accuracy of Kriging correlations.



(a) The Brinell hardness at the experimental No. 12



(b) The roughness profile at the experimental No. 12

Fig. 4. Representative results of the roller burnishing operation

Table 5. Experimental data for the roller burnishing process

No.	S (rpm)	f (mm/min)	D (mm)	AR (μm)	BH (HB)
Experimental data for training of the Kriging models					
1	400	300	0.04	0.41	348
2	1200	300	0.04	0.43	402
3	800	300	0.08	0.26	379
4	400	300	0.12	0.29	408
5	1200	300	0.12	0.32	519
6	800	300	0.08	0.24	376
7	800	100	0.04	0.28	382
8	800	500	0.04	0.41	315
9	800	100	0.12	0.17	484
10	800	300	0.08	0.25	377
11	800	500	0.12	0.29	391
12	400	100	0.08	0.32	365
13	400	500	0.08	0.45	298
14	800	300	0.08	0.26	378
15	1200	100	0.08	0.35	461
16	1200	500	0.08	0.48	367
17	800	300	0.08	0.27	375
Experimental data for testing accuracy of the Kriging models					
18	500	200	0.06	0.33	356
19	700	400	0.07	0.35	337
20	900	350	0.09	0.24	391
21	1100	300	0.11	0.28	473
22	900	250	0.05	0.31	378
23	1000	250	0.09	0.27	425
24	800	200	0.11	0.19	447

Table 6. The values of Kriging model parameters

Performance measures	Correlative parameter θ_i			Scalar factor β
	S	f	D	
AR	0.427254	0.246521	0.285591	0.085432
SH	0.174918	0.320256	0.737769	0.338244

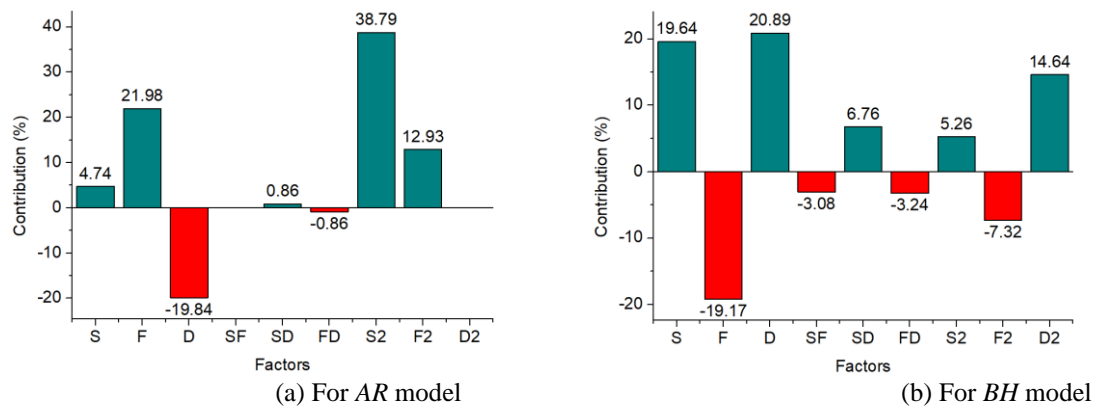


Fig. 5. Parametric contributions for the AR and BH models

Table 7. Computed ANOVA results for the AR model

Source	Sum of Squares	Mean Square	F Value	p-value	Contribution (%)
Model	0.10838	0.01204	24.92864	< 0.0001	
S	0.51168	0.51168	1066.00777	< 0.0001	4.74
f	2.37274	2.37274	4943.21746	< 0.0001	21.98
D	2.14173	2.14173	4461.93969	< 0.0001	19.84
Sf	0.00000	0.00000	0.00000	1.0000	0
SD	0.09284	0.09284	193.41069	0.756	0.86
fD	0.09284	0.09284	193.41069	0.756	0.86
S ²	4.18739	4.18739	8723.72181	< 0.0001	38.79
f ²	1.39580	1.39580	2907.90727	< 0.0001	12.93
D ²	0.00000	0.00000	0.00000	1.0000	0
Residual	0.00242	0.00048			
Cor Total	0.11080				
$R^2 = 0.9782$; Adjusted. $R^2 = 0.9702$; Pred. $R^2 = 0.9672$					

Table 8. Computed ANOVA results for the BH model

Source	Sum of Squares	Mean Square	F Value	p-value	Contribution (%)
Model	47962.71909	5329.19101	29.31302	0.0001	
S	20192.37831	20192.37831	111.06745	< 0.0001	19.64
f	19709.15949	19709.15949	108.40952	< 0.0001	19.17
D	21477.53478	21477.53478	118.13640	< 0.0001	20.89
Sf	3166.62552	3166.62552	17.41791	0.0038	3.08
SD	6950.12614	6950.12614	38.22892	< 0.0001	6.76
fD	3331.12555	3331.12555	18.32274	0.0036	3.24
S ²	5407.93839	5407.93839	29.74617	< 0.0001	5.26
f ²	7525.87624	7525.87624	41.39581	< 0.0001	7.32
D ²	15051.75247	15051.75247	82.79162	< 0.0001	14.64
Residual	909.01424	181.80285			
Cor Total	48871.73333				
$R^2 = 0.9814$; Adjusted. $R^2 = 0.9754$; Pred. $R^2 = 0.9646$					

Table 9. Testing results for developed Kriging models

No.	AR			BH		
	Experiment	Kriging	ER (%)	Experiment	Kriging	ER (%)
18	0.33	0.34	−3.03	356	358	−0.56
19	0.35	0.34	2.86	337	339	−0.59
20	0.24	0.25	−4.00	391	389	0.51
21	0.28	0.29	−3.45	473	471	0.42
22	0.31	0.32	−3.13	378	376	0.53
23	0.27	0.28	−3.57	425	428	−0.71
24	0.19	0.18	5.26	447	449	−0.45

4.2. PARAMETRIC INFLUENCES

As shown in Fig. 6a, it can be stated that the spindle speed has contradictory impacts on the surface roughness. When the speed changes from 400 to 800 rpm, the *AR* is decreased by 31.4%. When the speed increases from 800 rpm to 1200 rpm, the *AR* is increased by 54.2%. A higher speed leads to reductions in the hardness and strength of the workpiece due to higher temperature. The material is softly compressed; hence, the roughness decreases. Excessive speed may increase the vibration, resulting in an unstable burnishing operation; hence, the roughness decreases.

As shown in Fig. 6b, it can be stated that the surface roughness increases (relatively around 66.6%) with an increment in the feed rate (from 100 to 500 mm/min). At a low feed rate, the distance between burnishing paths decreases and the tool-tip flat abnormalities, leading to a reduction in the roughness. An increased feed rate causes larger feed marks between burnishing traces; hence the surface roughness increases. As a result, a low feed rate is a better selection for minimizing surface roughness due to the greater impact of the burnishing tool and regular metal flow.

As shown in Fig. 6c, it can be stated that the surface roughness decreases (relatively around 38.7%) with an increment in the burnishing depth (from 0.04 to 0.12 mm). A higher depth increases the burnishing pressure and the material is hardly burnished. The peaks are flattened and the valleys are filled; hence, the roughness decreases.

The interactive impacts of process inputs on the *AR* model are shown in Fig. 7.

As shown in Fig. 8a, it can be stated that the *BH* increases (relatively around 24.6%) with an increased *S* (from 400 to 1200 rpm). A higher speed increases the machining frequency and the number of burnishing traces, leading to work hardening; hence, the *BH* decreases.

As shown in Fig. 8b, it can be stated that an increased higher *f* (from 100 to 500 mm/min) decreases the *SH* (relatively around 20.1%). At a low feed rate, the number of burnishing traces increases and the material is extensively treated; hence, higher hardness is obtained. A higher feed rate decreases the processing time; hence, the *BH* decreases.

As shown in Fig. 8c, it can be stated that an increased *D* (from 0.04 mm to 0.12 mm) leads to a lower *SH* (relatively around 24.6%). A low depth decreases the burnishing pressure,

leading to a low degree of plastic deformation; hence, the *BH* decreases. A higher depth increases the degree of plastic deformation; hence, higher *BH* is obtained.

The interactive impacts of process inputs on the *BH* model are shown in Fig. 9.

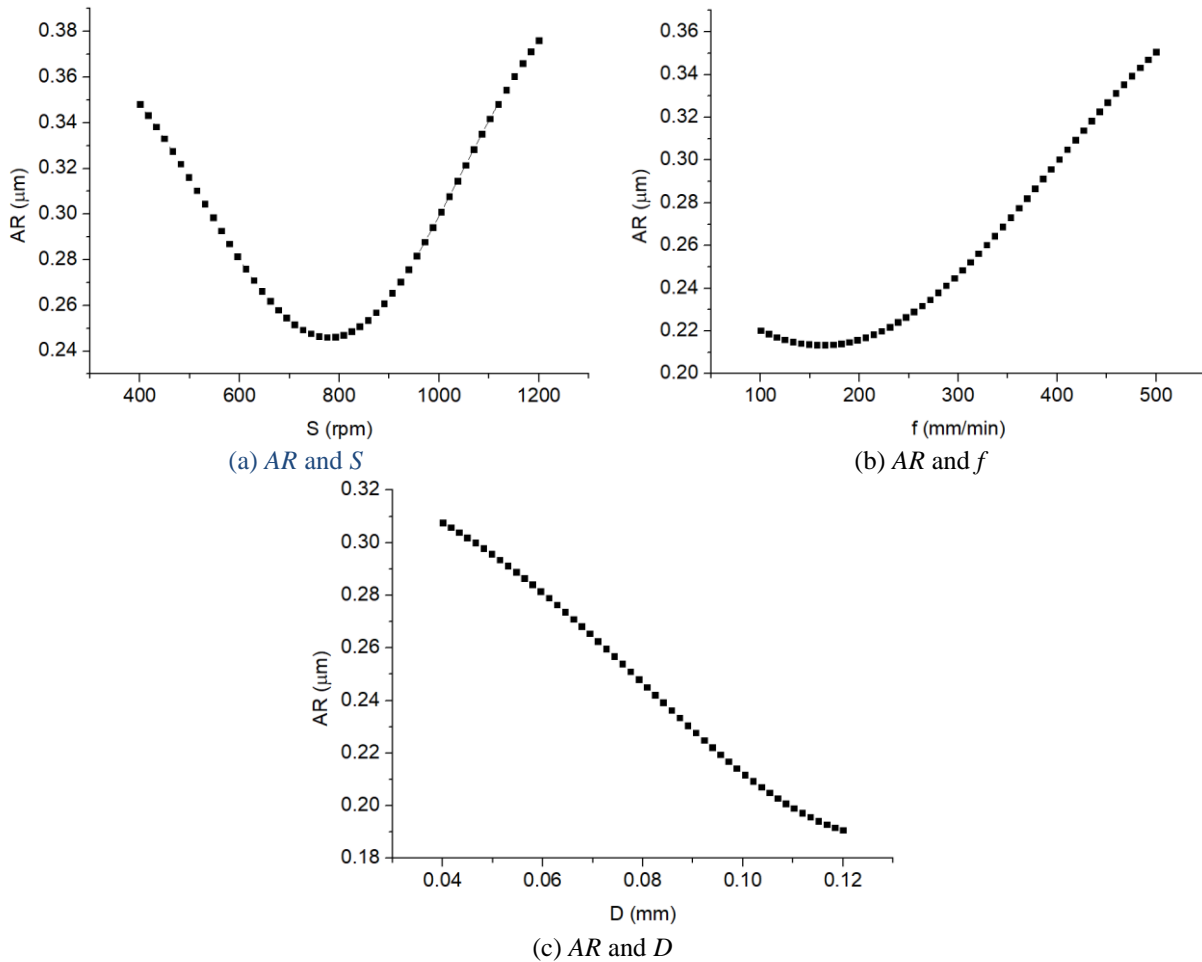


Fig. 6. The impacts of process parameters on the *AR* model

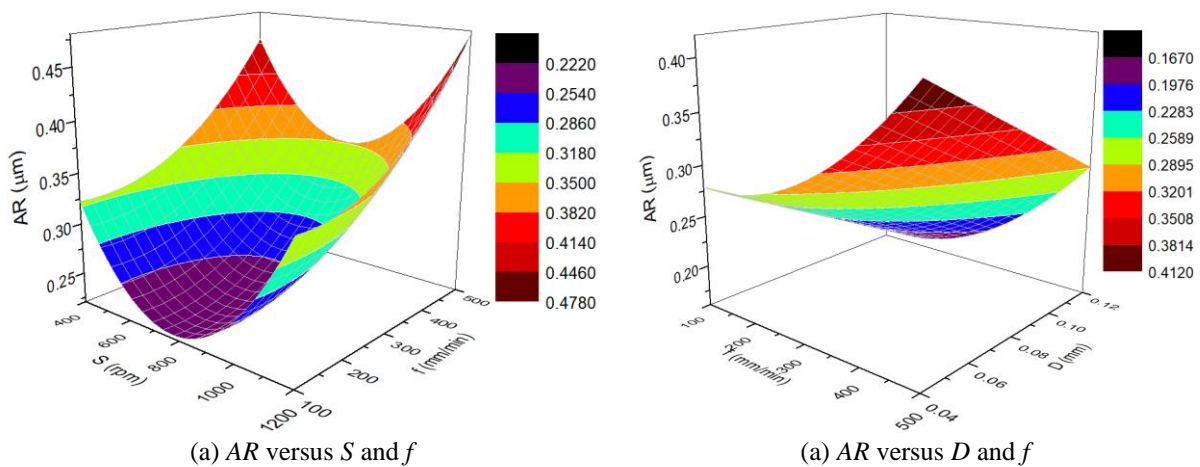


Fig. 7. The interactive impacts for the *AR* model

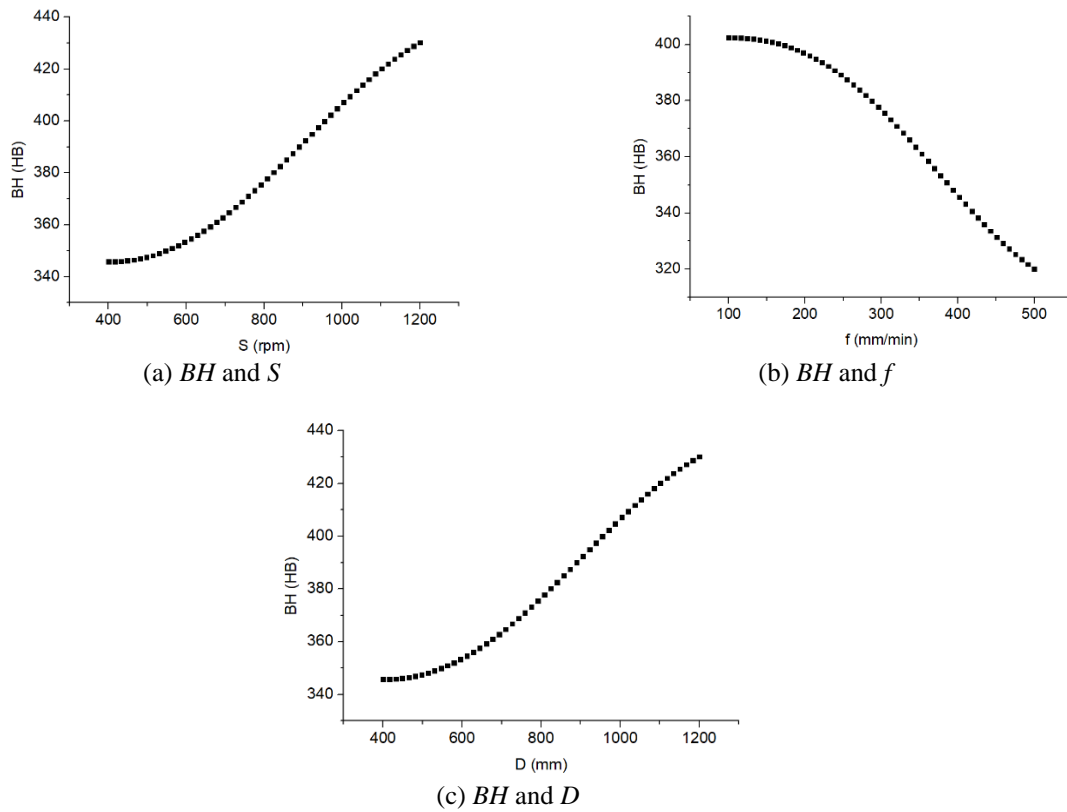


Fig. 8. The impacts of process parameters on the *BH* model

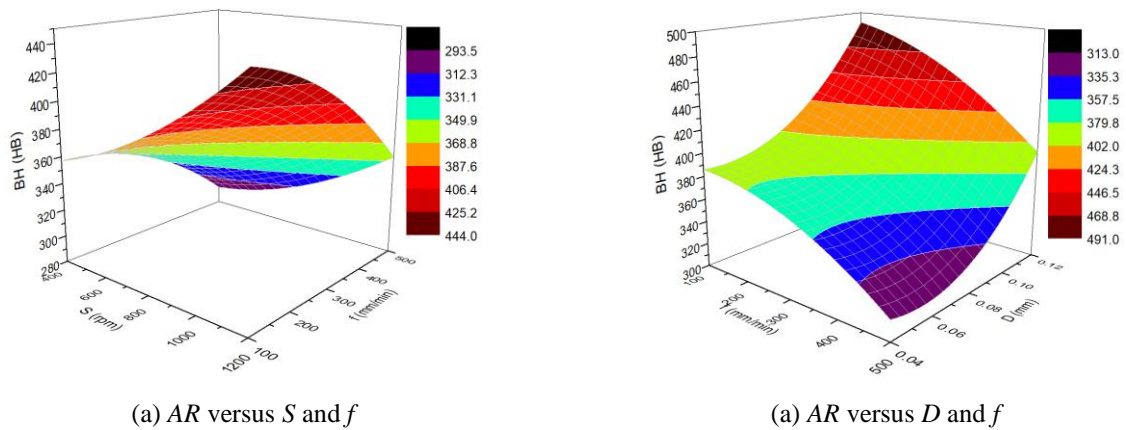


Fig. 9. The interactive impacts for the *BH* model

4.3. OPTIMIZING OUTCOMES GENERATED BY THE KRIGING MODELS-CSA

The optimizing issue is expressed as:

Minimizing *AR* and maximizing *BH*;

Constraints: $400 \leq S \leq 1200$ rpm; $100 \leq f \leq 500$ mm/min; $0.04 \leq D \leq 0.12$ mm.

The Pareto fronts produced by the CSA are shown in Fig. 8. It can be stated that a higher *BH* (a desired indicator) leads to a higher *AR* (a worsened indicator). As a result, the optimizing values of the *S*, *f*, and *D* are 832 rpm, 112 mm/min, and 0.12 mm, respectively (Table 10). The *AR* is decreased by 37.0%, while the *BH* is increased by 29.9% at the optimal point.

Table 11 presents the comparison between the pre-machined and burnished surfaces. As a result, the *AR* is decreased by 94.1% and the *BH* is enhanced by 77.1%, as compared to the milled surface. It can be stated that the roller burnishing process significantly decreases the surface roughness and improves the surface hardness. The burnishing pressure helps to decrease the irregularities on the milled surface, while the valley is filled up. Moreover, this helps to produce plastic deformation, which increases the hardness of the surface layer. In other words, the surface properties of the burnished surface sharply enhance.

Table 10. Optimizing outcomes

Methods	Optimization parameters			Responses	
	<i>S</i> (rpm)	<i>f</i> (mm/min)	<i>D</i> (mm)	<i>AR</i> (μm)	<i>BH</i> (HB)
Initial values	800	300	0.08	0.27	375
Optimal values	832	112	0.12	0.17	487
Reductions (%)				-37.0	29.9

Table 11. Comparison between the pre-machined and burnished surfaces

Machining methods	Burnishing responses	
	<i>AR</i> (μm)	<i>BH</i> (HB)
Milling	2.86	275
Burnishing	0.17	487
Improvement (%)	-94.1	77.1

4.4. SCIENTIFIC AND INDUSTRIAL CONTRIBUTIONS

The scientific and industrial contributions are expressed as:

The proposed optimizing technique can be efficiently applied to find global results for not only other burnishing operations but also machining processes.

The nonlinear experimental data can be presented using the Kriging approach.

The optimal data of the burnishing inputs and responses can be obtained using the Pareto graphs produced by the CSA (Fig. 10).

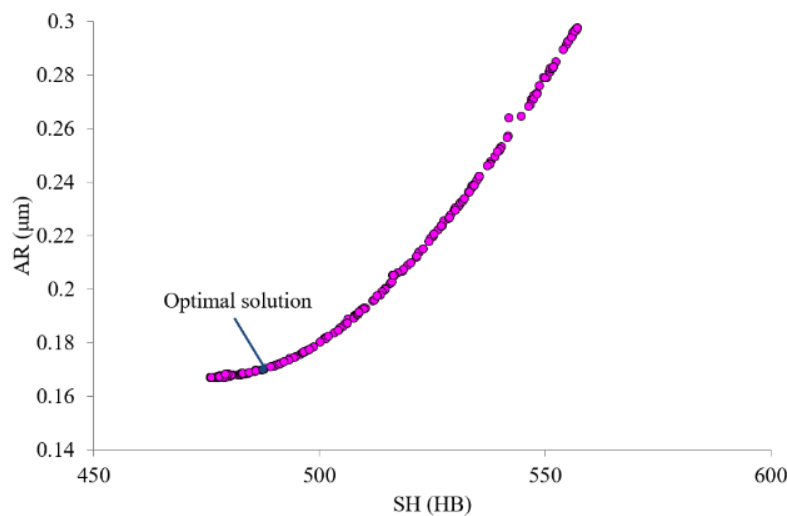


Fig. 10. The Pareto front produced by the CSA

The Kriging-based AR and BH models can be applied to forecast the burning responses in the practice.

The performance measures can be significantly enhanced using optimal outcomes.

5. CONCLUSIONS

This study addressed the roller burnishing operation of the hardened steel and optimized the process inputs (the spindle speed, feed rate, and depth of penetration) to decrease the average roughness and Brinell hardness. The correlative models of the performance measures were proposed using the Kriging approach, while optima were found using the CSA. The obtained outcomes are expressed as:

1. Higher speed and depth were applied to improve the Brinell hardness, while a low feed rate was recommended. Low speed and feed rate were utilized to obtain a smoother surface, while a high depth was recommended.

2. The feed rate was to be found to be the most effective input for the roughness model, followed by the depth and speed. The depth was to be found to be the most effective input for the hardness model, followed by the speed and feed rate.

3. The optimal findings of the speed, feed rate, and depth were 832 rpm, 112 mm/min, and 0.12 mm, respectively. The enhancements in the *AR* and *BH* were 29.9% and 37.0%, respectively.

4. This work addressed the surface properties under variation of process parameters. The machining costs and energy consumption will be addressed in future works.

REFERENCES

- [1] STALIN JOHN M.R., BANERJEE N., SHRIVASTAVA K., VINAYAGAM B.K., 2017, *Optimization of Roller Burnishing Process on EN-9 Grade Alloy Steel Using Response Surface Methodology*, J. Braz. Soc. Mech. Sci. Eng., 39, 30893101.
- [2] PATEL K.A., BRAHMBHATT P.K. 2018, *Response Surface Methodology Based Desirability Approach for Optimization of Roller Burnishing Process Parameter*, J. Inst. Eng. India Ser. C 99, 729–736.
- [3] STALIN JOHN M.R., BALAJI B., VINAYAGAM B.K., 2017, *Optimisation of Internal Roller Burnishing Process in CNC Machining Center Using Response Surface Methodology*, J. Braz. Soc. Mech. Sci. Eng. 39, 4045–4057.
- [4] YUAN X.L., SUN Y.W., GAO L.S., JIANG S.L., 2016, *Effect of Roller Burnishing Process Parameters on the Surface Roughness and Microhardness for TA2 alloy*, Int. J. Adv. Manuf. Technol., 85, 1373–1383.
- [5] SHANKAR E., BALASIVANANDHA PRABU S., SAMPATH KUMAR T., STALIN JOHN M.R., 2018, *Investigation of TiAlN Coated Roller Burnishing on Al-(B4C)p MMC Workpiece Material*, Mater. Manuf. Process., 33/11, 1242–1249.
- [6] NGUYEN T.T., LE X.B., 2018, *Optimization of Interior Roller Burnishing Process for Improving Surface Quality*, Mater. Manuf. Process., 33/11, 1233–1241.
- [7] NGUYEN T.T., 2021, *Multi-Response Performance Optimization of Burnishing Operation for Improving Hole Quality*. J. Braz. Soc. Mech. Sci. Eng., 43, 560.
- [8] NGUYEN T.T., LE M.T., 2021, *Optimization of Internal Burnishing Operation for Energy Efficiency, Machined Quality, and Noise Emission*, Int. J. Adv. Manuf. Technol., 114, 2115–2139.
- [9] NGUYEN T.T., NGUYEN T.A., TRINH Q.H. LE, X.B., PHAM L.H., LE, X.H., 2022, *Artificial Neural Network-based Optimization of Operating Parameters for Minimum Quantity Lubrication-Assisted Burnishing Process in Terms of Surface Characteristics*, Neural Comput. & Applic., 34, 7005–7031.
- [10] DUNCHEVA G.V., MAXIMOV J.T., DUNCHEV V.P., ATANASOV T.P., CAPEK J., 2020, *Single Toroidal Roller Burnishing Of 2024-T3 Al Alloy Implemented as Mixed Burnishing Process*, Int. J. Adv. Manuf. Technol., 111, 3559–3570.

- [11] NGUYEN T.T., NGUYEN T.A., TRINH Q.H., LE X.B., 2022, *Multi-Performance Optimization of Multi-Roller Burnishing Process in Sustainable Lubrication Condition*, Mater. Manuf. Process., 37/4, 407–427.
- [12] PRASAD K.A., JOHN, M.R.S., 2021, *Optimization of External Roller Burnishing Process on Magnesium Silicon Carbide Metal Matrix Composite using Response Surface Methodology*. J. Braz. Soc. Mech. Sci. Eng., 43, 342. <https://doi.org/10.1007/s40430-021-03069-3>.
- [13] LE V.A., NGUYEN T.T., 2022, *Investigation and Optimization of MQL System Parameters in the Roller-Burnishing Process of Hardened Steel*, Stroj. Vestn./J. Mech. Eng., 68/3, 155–165.
- [14] HOANG TIEN D., TRUNG D.D., VAN THIEN N., NGUYEN N., 2021, *Multi-Objective Optimization of the Cylindrical Grinding Process of SCM440 Steel Using Preference Selection Index Method*, J. Mach. Eng., 21/3, 110–123, <https://doi.org/10.36897/jme/141607>.
- [15] DANG T.X., SON N.H., CUONG P.D., 2022, *Research on Optimizing Spray Parameters for Cr₃C₂ – NiCr Coating Created on Alloy Steel by Plasma Spraying Technique*, J. Mach. Eng., 22/4, 43–53, <https://doi.org/10.36897/jme/157047>.